Classification of ash spectra in various environmental settings

Martin Okánik

August 2021

supervisors: Dr Isabelle Taylor, Professor Roy Grainger

Acronyms used:

- BT - brightness temperature
- BTS - brightness temperature spectrum
- LUT - look-up table
- ML - machine learning
- NN - neural network
- TIR - thermal infrared

1 Introduction and background

The goal of this project is to build a machine learning (ML) model to classify the thermal infrared (TIR) volcanic ash spectra based on their chemical composition. Satellite observations of post-eruption volcanic plumes are easily accessible (instruments such as IASI carried on the MetOp satellites). However, not all eruptions sites are quickly and easily accessible for the collection of physical samples of the ash material. Different chemistry of erupted material is clearly manifested in the spectra, so one could deduce the chemical composition based on inspection of TIR spectra. The spectra can also vary with emissivity properties of the underlying surface and radiative transfer in the atmospheric column. This is a multi-dimensional problem, and it seems promising to employ ML methods to tackle its complexity.

For this reason, we have run numerous radiative transfer calculations to create as wide dataset as possible. The next step was to train an ML algorithm over the (reduced) dataset and examine its performance on real world data.

1.1 Volcanic ash

Volcanic ash consists of fragments of volcanic minerals, rocks and glass, in size range of roughly 0.004 mm to 2 mm (adopting the definition of Volcanic Ashfall Impacts Working group in the US: `https://volcanoes.usgs.gov/volcanic_ash/ash.html`). Its composition is directly related to that of magma and to some extent to the eruption type. From the other perspective, it is possible to trace an ash sample to a particular eruption, provided that something is already known about the eruption itself - some sample already collected. Sometimes, this does not need to be the current eruption, but one of the previous eruptions.

Chemical composition of the ash is usually expressed in the silica content - alkali content plane, see Figure (1) This also correlates with the eruption mode of the volcano.

For the simulations, 17 ash types were used. These ash types are tabulated among other variable parameters in Table (1). In this context, the term "ash type" refers to a specific model for the complex refractive index of a particular ash sample from a previously studied eruption. These refractive indices were used in the radiative transfer calculations and hence produced different modifications to a theoretical clear sky spectrum.

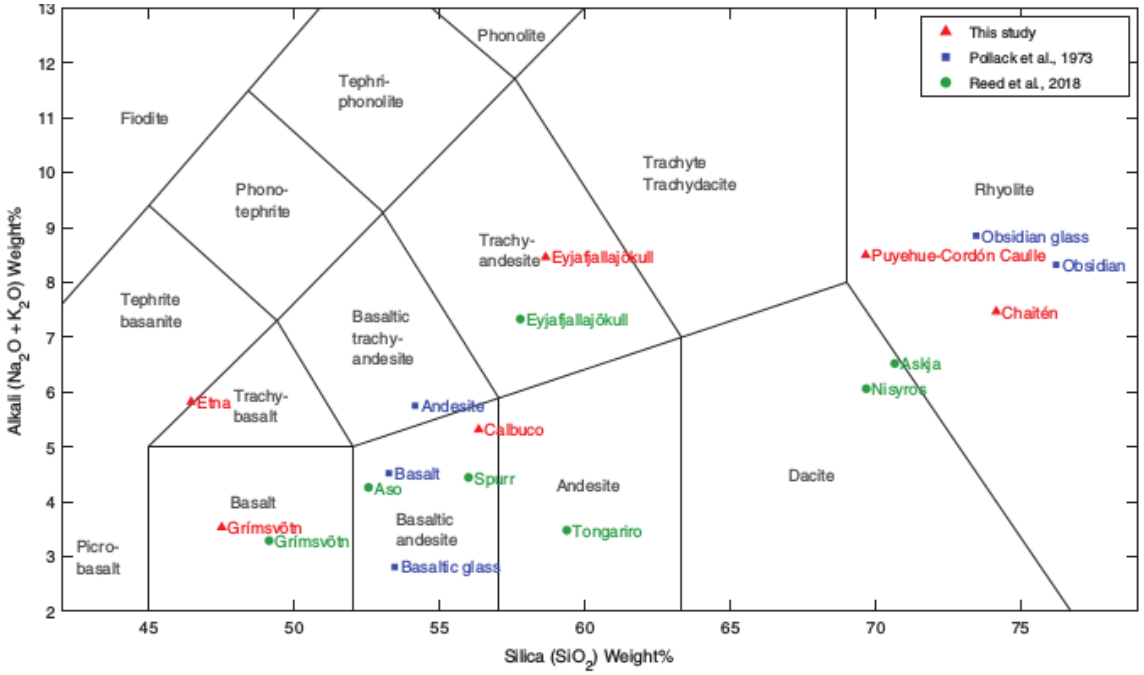

Figure 1: Chemical composition of various ash types, many of them used in this work. Taken from: Deguine et al. (2020)

1.2 Previous studies and the context of this work

Rise of ML in recent years motivated multiple scientific teams to try using this technique to study volcanic ash. Shoji et al. (2018) have used neural networks to classify eruption types, with more emphasis on volcanologic parameters and geometric properties of ash particles. Unlike this study, we adopted an approach more sensitive to atmospheric variations and explored a wide range of environmental conditions. Picchiani et al. (2011) classified the data as ash/non-ash with great accuracy, and were able to estimate the mass of ash, if present. Our approach relied on using a very wide artificial dataset to distinguish ash type variations disguised in a wide range of other variations. A noteable study was done by Ishimoto et al. (2021), which was in the preprint at the time of writing this report. Authors fitted the TIR spectra of multiple volcanic eruptions with 21 refractive index models by minimizing the brightness temperature (BT) difference between measurements and simulations (based on these refractive indices). In some (yet not all) cases, the inferred optimal refractive indices corresponded precisely to ones determined in the laboratory, based on volcanic ash samples from the same volcanic eruption events.

More information on the current state of ML in volcanology can be found in the review of Carniel et al. (2020). Our work has not relied on and was not directly motivated by the previously cited papers. We adopted an approach from scratch, using very simple ML approaches and available libraries (scikit-learn: to explore the possibilities of ash classification in changing environmental settings.

2 Creating the dataset

The shape of TIR brightness temperature spectrum (BTS) depends on ash type, atmospheric profile, pressure corresponding to the vertical position of ash cloud in the atmospheric column, its quantity (optical depth) and particle size, and surface properties: surface emissivity spectrum and temperature. Each of these is outlined in Table (1). Plots of these can be viewed for reference in the appendix. Atmospheric profiles and emissivity spectra can be seen in Figure (6) and Figure (7), respectively. All ash types are plotted for a fixed set of remaining parameters in Figure (8). Partial variations with respect to the four scalar parameters are included in Figure (9). Ranges of suitable values were generally taken from typical values found in previous research, mainly Ventress et al. (2016).

Property	Values	Description
type of volcanic ash (17x)	refractive index models from previous eruptions, including Grimsvotn, Askja, Mayon, Etna, Nisyros, Calbuco, Aso, Spurr, Eyjafjallajokull, Tongariro, Chaiten... See Table (2) for an explicit listing of these, also with class labels.	complex refractive index is tabulated for each wavenumber for which radiative transfer calculation is made, describes the interaction of TIR radiation with ash particles and is a major factor in determination of the resulting spectral shape. See Deguine et al. (2020) and Reed et al. (2018) for more on tabulation of complex refractive indices.
type of atmospheric profile (6x)	stn - standard atmosphere day - day in mid-latitudes ngt - night in mid-latitudes eq - equatorial sum - polar summer win - polar winter	atmospheric profile also enters into radiative transfer to determine the background clear spectrum (i.e. with no ash). This also has influence on spectral lines from atmospheric gases, which is independent of ash type and thus unimportant for ash classification
type of surface emissivity spectrum (6x)	snow ice seawater grass sand soil	tabulated for each simulated wavenumber, also determines the shape of background clear spectrum, obtained from MODIS UCSB Emissivity Library by interpolation of published spectra (and, at times, averaging over a few samples). This database was collected by Dr. Zhengming Wan's Group at ICESS and can be found at `https://icess.eri.ucsb.edu/modis/EMIS/html/em.html`.
ash optical depth (10x)	[10, 5, 2.5, 1.25, 0.625, 0.3125, 0.156, 0.078, 0.039, 0.0195]	scalar quantity giving the total amount of ash in a vertical column
effective radius in μm (8x)	[0.2, 0.4, 0.8, 1.6, 2.4, 3.2, 4.0, 8.0]	scalar quantity giving the radius of spheres with same volume as (non-spherical) ash aerosol particles
pressure at plume height in mb (5x)	[100, 250, 400, 750, 900]	scalar quantity placing the ash layer in the atmospheric profile defined above
surface temperature in K (5x)	[240, 260, 280, 300, 320]	scalar quantity influencing the clear spectrum

Table 1: Description of the entire parameter space for creating the dataset for machine learning.

Class label	LUT name
0	A83
1	AshMayon_patterson_1975
2	H2SO4_75_Palmer_1975
3	ICE235_Zasetsky_2005
4	askja_ash_Reed
5	aso_ash_Reed
6	calbuco_ash_Deguine_2020
7	chaiten_ash_Deguine_2020
8	etna_ash_Deguine_2020
9	eyjafjallajokull_ash_Deguine_2020
10	eyjafjallajokull_ash_Reed_2
11	eyjafjallajokull_ash_Reed
12	grimsvotn_ash_Deguine_2020
13	nisyros_ash_Reed
14	puyehue-cordon-caulle_Deguine_2020
15	spurr_ash_Reed
16	tongariro_ash_Reed

Table 2: List of the 17 complex refractive index look-up tables (LUTs) that were used for training of ML model. 15 of these correspond to volcanic ash, while two represent sulphur dioxide and ice. Integers in left column correspond to classes as they are labeled in the model.

2.1 Radiative transfer model and the execution of simulations

RTTOV radiative transfer model (`https://nwp-saf.eumetsat.int/site/software/rttov/`) was used for simulating the TIR spectrum in the space of parameters described above. A separate simulation was performed for each ash type, atmospheric profile and surface emissivity. Inside each simulation, the remaining four quantities from Table (1) were looped over. This amounts to $10 \times 8 \times 5 \times 5 = 2000$ spectra for each simulation file, and $2000 \times 17 \times 6 \times 6 = 1224000$ spectra in total. Simulations were performed on the cluster of the Department of Atmospheric, Oceanic and Planetary Physics (AOPP) at Oxford University, and their output was stored in .sav files. The scripts calling the simulations were in IDL, while the simulation code itself was in FORTRAN. The main simulation output was, for each spectrum, an array of brightness temperature data for each of 2401 channels in the wavenumber range of [800, 1400] cm^{-1}.

2.2 Creating the input files

Brightness temperature and ash type data were extracted from the .sav files which stored the simulation output. A text file *spectra* was created, which stores an array of shape $[N, m]$, N being the number of spectra and m being the number of channels in each spectrum. This means that there are N training examples (disregarding train-test split, for now) and each of them is constituted by a flat vector of m brightness temperature data.

Ash types were extracted into an array of shape $[m, 1]$. Each individual ash type was mapped into an integer $0 - 16$ and this was stored in a text file *labels_int*, which fed in the labels for the ML algorithm.

3 Machine learning

3.1 Neural Networks

ML algorithm chosen for this purpose was the neural network (NN). NN consists of an input layer, an output layer, and one or more hidden layers in between, see Figure (2). Input data (spectra) and their scalar integer labels are fed into the NN at input layer, which has dimensions $[m, 1]$. Output layer displays the prediction. NN works by taking a weighted sum of all entries (neurons) in the preceding layer (starting with the input layer), applying a non-linear decision function to this number, and assigning it to the corresponding neuron in the next layer. Each neuron in $i+1$-th layer is generated from all neurons

in i-th layer by a matrix multiplication of i-th layer with a distinct set of coefficients. These coefficients are then "learned" (i.e. chosen) by minimizing a cost function. Cost function quantifies the degree of mismatch between the model and real values (labels). The ability of ML algorithms, NN in particular, to learn complex tasks is due to the non-linearity of the decision function, which distinguishes the process of predicting a result from a sequence of (linear) matrix multiplications.

To assess the accuracy of the algorithm, one needs to look at the corresponding predicted and true labels and calculate the train set score and test set score. These scores quantify how large fraction of predicted labels coincides with the original true labels. The test set score is the significant metric for ML, as it captures how well the model copes with data it has never seen before. The train set score describes how well the trained coefficients capture and correctly describe the variability they were trained on. Hence train set score is normally a bit larger than test set score, due to tendency of model coefficients to adjust to random noise in the data and interpret these minor trends as part of the intrinsic (functional) variability. This is called overfitting and can be diagnosed by a large disparity between the train set score and test set score. Regularization is a procedure to limit overfitting. Roughly speaking, it penalizes large coefficients by adding them to the cost function. This makes the the ML algorithm converge to a new optimum in the set of coefficients, in a way that it only preserves the truly important variations, and filters out the noise. By drawing an analogy with a simple regression in 2D plane, this would typically correspond to putting more emphasis on the lower powers in some polynomial fitting function.

Vast and rich literature is available for learning about NNs and other ML algorithms, from theoretical aspects to direct applications to data. For the purposes of this internship and this report, the book "Introduction to Machine Learning in Python" by Muller&Guido (see references) and the Coursera course by Andrew Ng on ML (found at `https://www.coursera.org/learn/machine-learning/home/welcome`) were used as reading/study materials.

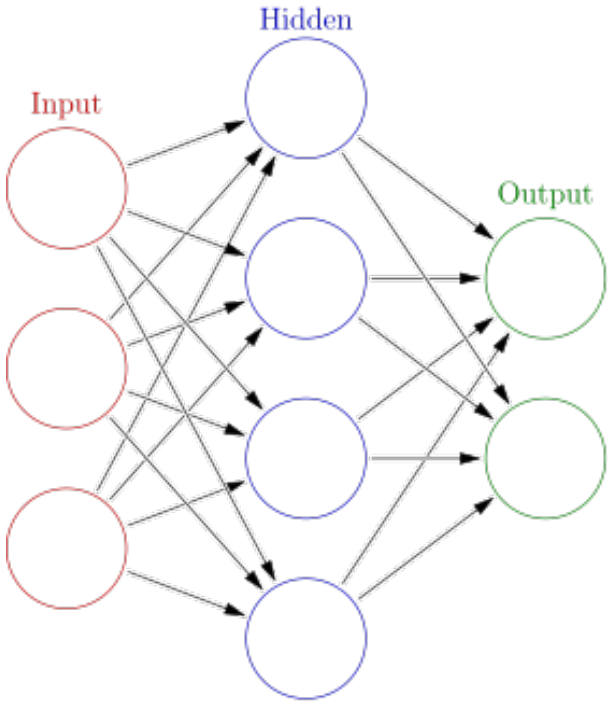

Figure 2: A simple illustration of a neural network. Each arrow represents a coefficient. Unlike in this picture, the neural network used in this work calculated only one output. Taken from: `https://en.wikipedia.org/wiki/Artificial_neural_network`

3.2 Preparation for training and dataset adjustment

The package used was scikit-learn, in particular the mlp function. MLP stands for multi-layer perceptron, which is a more formal term for NN. scikit-learn handles the train-test split automatically. This means that input data points are randomly shuffled and split into the train set (used for training the coeficients of the NN) and the test set (preserved to still have unused data for an unbiased evaluation of model

performance). The default ratio of 80:20 of train/test sets was adopted throughout. One hidden layer was used throughout this study, and the number of neurons in it was set to be one half of the number of input neurons (the number of spectra). Each channel in a spectrum was treated as one of m features of that training example (out of N spectra/training examples).

The full dataset of $> 10^6$ spectra, each of $> 10^3$ channels proved to be too large for our present purposes and equipment. Therefore we restricted this study to the surface emissivity type "seawater". This is also by far the most abundant surface type on Earth, and in itself includes a relevant population of volcanoes. In any realistic situation, we would know over which type of surface the volcanic ash was measured by the satellite from its coordinates, so this reduction does not have any serious consequences for the usefulness of our model. Further, we fixed the atmospheric profile type to "standard". Again, for a known geographical location and time of measurement, availability of meteorological data should allow us to specify only one atmospheric type. Removal of these two quasi-redundant "dimensions" reduces the required dataset by a factor of 36, to just 34,000 spectra. We still cover the full range of variations of ash optical depth, effective radius, pressure at plume height and surface temperature. By a similar reasoning to that above in this paragraph, surface temperature could be eliminated as well, in favour of more resolution in remaining parameters (presumed to be truly unknown). This should be addressed in the future.

When looking at Figure (6) or Figure (8), we see that the high-wavenumber part of the spectrum above roughly 1250 cm^{-1} features a very strong absorption. This is due to water vapour in the atmosphere. We removed this part of the spectrum to let the algorithm focus on channels which are more useful for distinguishing ash type. The final wavenumber range used was thus [800, 1250] cm^{-1}.

4 Results

4.1 Results: the reduced dataset (4 ash types)

Development of ML algorithm was done using a reduced dataset of 8000 spectra of 4 different ash types (fixed at standard atmosphere and the surface emissivity of seawater). The ash types used for this were from look-up tables named A83, AshMayon_patterson_1975 (naming convention describes volcano, author and year), H2SO4_75_Palmer_1975 and ICE235_Zasetsky_2005. The selection of these was random/alphabetical. Regularization parameter was increased from default 0.001 to 0.01, as the original model significantly overfitted the training set. The training took ∼30 minutes and achieved a train set score of 88 % and a test set score of 86 %. As the latter two file names imply, 2 out of 4 refractive indices corresponded to ice and sulphur dioxide, not ash. These spectra are quite specific, and while not completely standing out compared to ash spectra, some of their characteristics might have facilitated the learning and provided and overestimate of model performance.

For a better picture of classification of four spectra, we trained several models for different purposefully chosen quartets of ash types. Selection was based on increased or decreased visual likeness between the spectra. Results of different choices are presented in Table (3).

From the table, it is seen that the test set score is around 90% regardless of the choice of the quartet. It even seems that ash types deliberately chosen as visually similar reached the same performance that those deliberately different. This is contrary to what would be expected, as the core of our task is to *resolve* the spectra from each other. Also, neither ice nor sulfuric acid were resolved better than remaining spectra, which were composed of true volcanic ash.

4.2 Results: the full dataset (17 ash types)

Using the full range of 17 distinct ash types, and still fixing the surface emissivity type at "seawater" and atmospheric profile type at "standard", training of the full model was performed. When having 17 spectra, the test set score fell to 62%. This is not enough to be usable (in its current form) for a trustworthy chemical analysis of satellite TIR observations, but is still significantly better than than the $1/17 = 5.9\%$ reached by a random guess.

The confusion matrix for this model is plotted in Figure (3). Confusion matrix determines which datapoints (that have some known true label) are correctly/incorrectly classified with which labels. More precisely, the entry index (i, j) gives the absolute or relative occurrence of i-th true class predicted as j-th class. We hoped to see some physical signal in this matrix, i.e. chemically similar spectral types should be mistaken for each other far more frequently than ash labels that are not intrinsically similar to each other (e.g. from the same volcano, there are 3 different Eyjafjallajökull LUTs, as can be seen in Table

Keyword	Selected LUTs	Description	Test set score
basic	A83 AshMayon_patterson_1975 H2SO4_75_Palmer_1975 ICE235_Zasetsky_2005	original 4 described in the paragraph, first four in alphabetical order	87 %
near	eyjafjallajokull_ash_Reed etna_ash_Deguine_2020 A83 chaiten_ash_Deguine_2020	4 spectra visually chosen as the most similar to eachother	91 %
far	eyjafjallajokull_ash_Deguine_2020 ICE235_Zasetsky_2005 H2SO4_75_Palmer_1975 grimsvotn_ash_Deguine_2020	4 spectra visually chosen as the least similar to eachother	91 %
rnd1	puyehue-cordon-caulle_Deguine_2020 spurr_ash_Harbin_1995 spurr_ash_Reed tongariro_ash_Reed	alphabetical selection of the last quartet of spectra	90 %
rnd2	eyjafjallajokull_ash_Reed grimsvotn_ash_Deguine_2020 nisyros_ash_Longchamp_2011 nisyros_ash_Reed	alphabetical selection of the second last quartet of spectra	90 %
rnd3	chaiten_ash_Deguine_2020 etna_ash_Deguine_2020 eyjafjallajokull_ash_Deguine eyjafjallajokull_ash_Reed_2	alphabetical selection of the third last quartet of spectra	91 %

Table 3: Different selections of 4 spectral ash types, givens as look up tables (LUTs) for the wavenumber dependence of the complex refractive index correspponding to given ash type.

(2)). In other words, when i and j encode ash types that lie close to each other in a chemical composition plot such as Figure (1), the (i, j) component should be large. From the figure, it is clear that this does not happen. While most of the signal lies directly on the diagonal (i.e. correct classifications), only the elements near the diagonal have any non-negligible prediction rate. Integer indices encode the ash type in a random (alphabetical) way, so there is no physical reason why $j = i-1$ or $j = i+1$ should be predicted in any way more often than e.g. $j = i + 7$. It is clear that this is an undesirable computational artifact, coming probably from the way how the NN arrives at the desired integer label. It seems that, in virtually all cases, the computation "falls" roughly towards the desired label, but sometimes is misdirected by one or two integers in either direction. This is clearly a sub-optimal, or even incorrect way of doing multiple-class classification (number of classes is 17 in our case).

4.3 Results: many-dimensional label vectors

In an attempt to address the deficiency of ML model described above, another model was trained using different encoding of classes. Instead of integers from 0 to 16 to label the 17 ash types, 17-dimensional vectors (1, 0, ..., 0) to (0, 0, ..., 1) were used. It was believed that this could remove the problem of neighbouring integers and make every class, in an abstract sense, "equidistant" from all the other classes. This so far proved wrong, as can be seen in Figure (4). We had an additional complication of occurrences of non-classifications or double-classifications (i.e. 0 or 2 classes selected instead of 1). This complication can be addressed, but the artifact of "nearby integers" seemed to translate into that of "nearby dimensions", contrary to our expectations. A better way of doing multi-class classification is urgently needed for future work.

4.4 Results: application on real data

As a further test of our model, we applied it on real-world TIR spectra from one day of the 2010 Eyjafjallajökull eruption. The results can be found in Figure (5). Each dot represents an IASI pixel. In the figure, there are 19 classes instead of 17. This is because an earlier version of the model had 19 ash

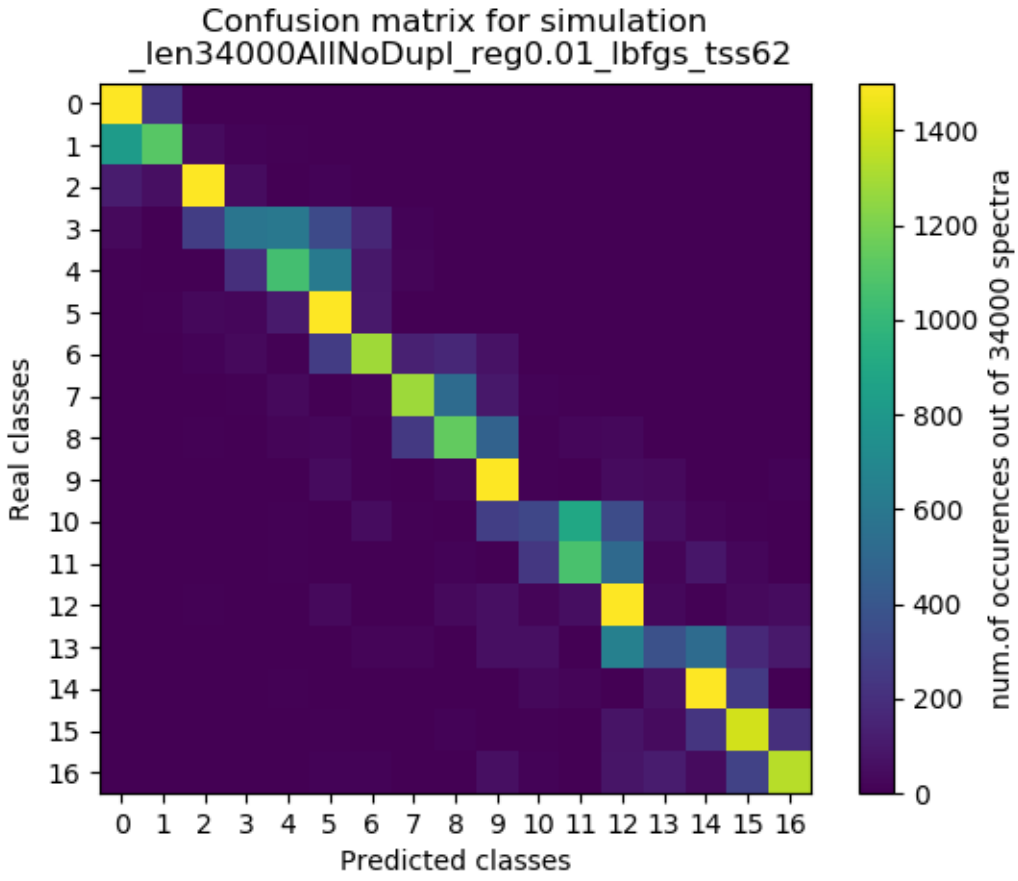

Figure 3: Confusion matrix for full model.The entry index (i, j) gives the absolute or relative occurrence of i-th true class predicted as j-th class. Classes are encoded as scalar integers 0-16, and correspond to different ash types, more concretely their tabulated complex refractive index spectra.

types, of which there were two duplicates. These were removed, bringing the number of classes to 17. The classes corresponding to the three Eyjafjallajökull erruptions are numbered 9 - 11, see also Table (2), this has not changed. None of the duplicates was a particularly favoured choice in this example, so our findings still hold. We can see that the expected labels are predicted only for a central stream of pixels within a few hundreds of kilometers from the volcano, but at the same time not too close (i.e. more than around 100 km). Edges of the south-going plume are misidentified to various other volcanoes. The most popular choice (including the correct Eyjafjallajökull LUTs 9-11) by far is Calbuco. It can be checked in Figure (5) that Calbuco is a relatively close neighbour to Eyjafjallajökull in the silica-alkali plane, in fact the closest neighbour out of the handful of important volcanoes that are depicted there. It is a basaltic andesite, while Eyjafjallajökull is a trachy-andesite, meaning that Calbuco has both lesser alkali and lesser silica content (i.e. it is more towards the basaltic edge of the graph). Another popular choice for the algorithm was ice (label 6). Both Calbuco ash and ice were predicted in large separated clouds thousands of kilometers southwest of the volcano. The third most popular misclassification was the ash from Mount Tongariro, mainly found at the edges of the plume hundreds of kilometers from the volcano, to the sides of the correctly classified Eyjafjallajökull pixels. Despite the inability of the model to correctly identify majority of pixels as Eyjafjallajökull, it is reassuring to know that most of the misclassifications were with volcanoes that are, in terms of our sample, neighbours in chemical composition. It is possible that this misclassification into neighbouring chemical compositions is the "signal" that we struggled to find in artificial datasets, and which serves as a sanity check of our results.

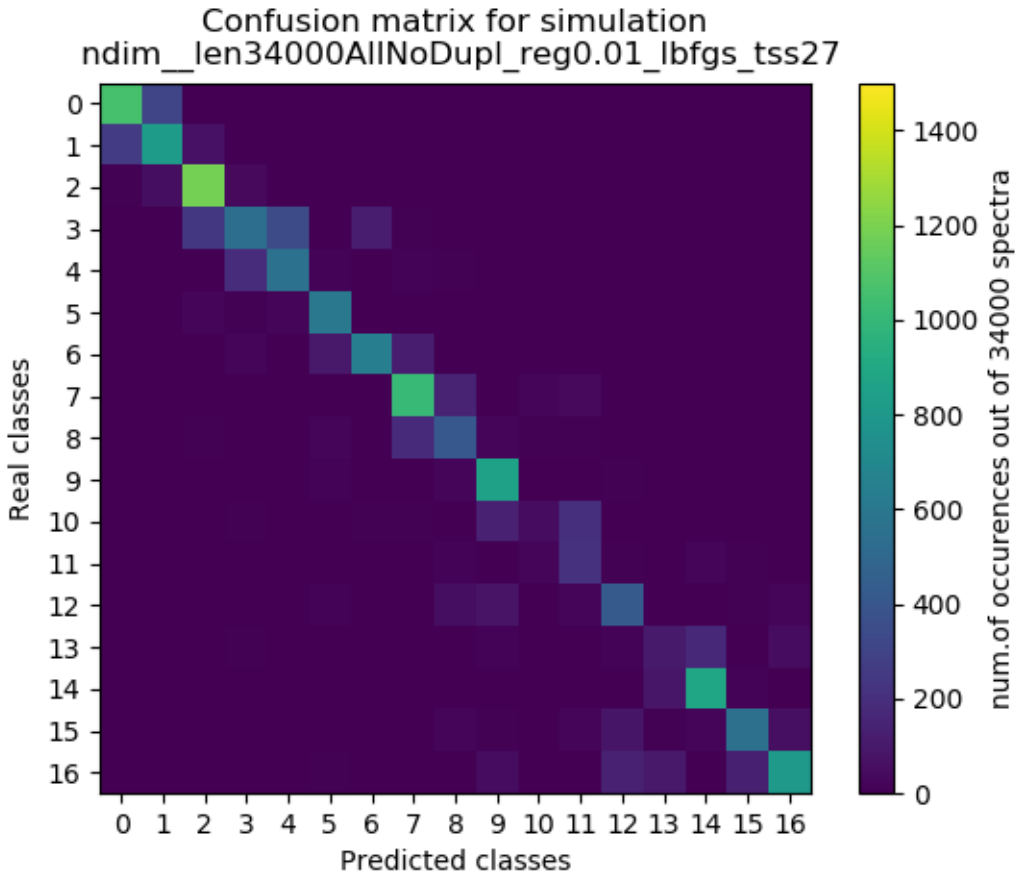

Figure 4: Confusion matrix for full model, using a 17-dimensional label, where e.g. (0, 0, 1, .. 0) represents the class 2 etc. In the plot, the entry index (i, j) gives the absolute or relative occurrence of i-th true class predicted as j-th class. Classes are encoded as scalar integers 0-16, and correspond to different ash types, more concretely their tabulated complex refractive index spectra.

5 Conclusions and further work

Our results indicate that using ML for classifying ash type, when some of the environmental and geometrical settings are unknown, might be a promising endeavour. There remains a lot of work to be done, in particular:

- try other ML algorithms:

  Neural Networks are a very powerful algorithm for their capacity to learn complex tasks, but it might be worthwhile to try other ones to see if they can perform comparably well, at possibly shorter training time.

- optimize settings of neural network:

  Regularization parameter was tuned to bring test set score close to train set score. There are many other parameters of scikit-learn mlp function that could be tuned to see whether algorithm's performance might increase. At present, training the model takes a very long time, so appropriate exploration of the parameter space was not completed.

- optimize parameter ranges for the particular task:

  Different real-life applications will require carefully constructed datasets. It should be decided

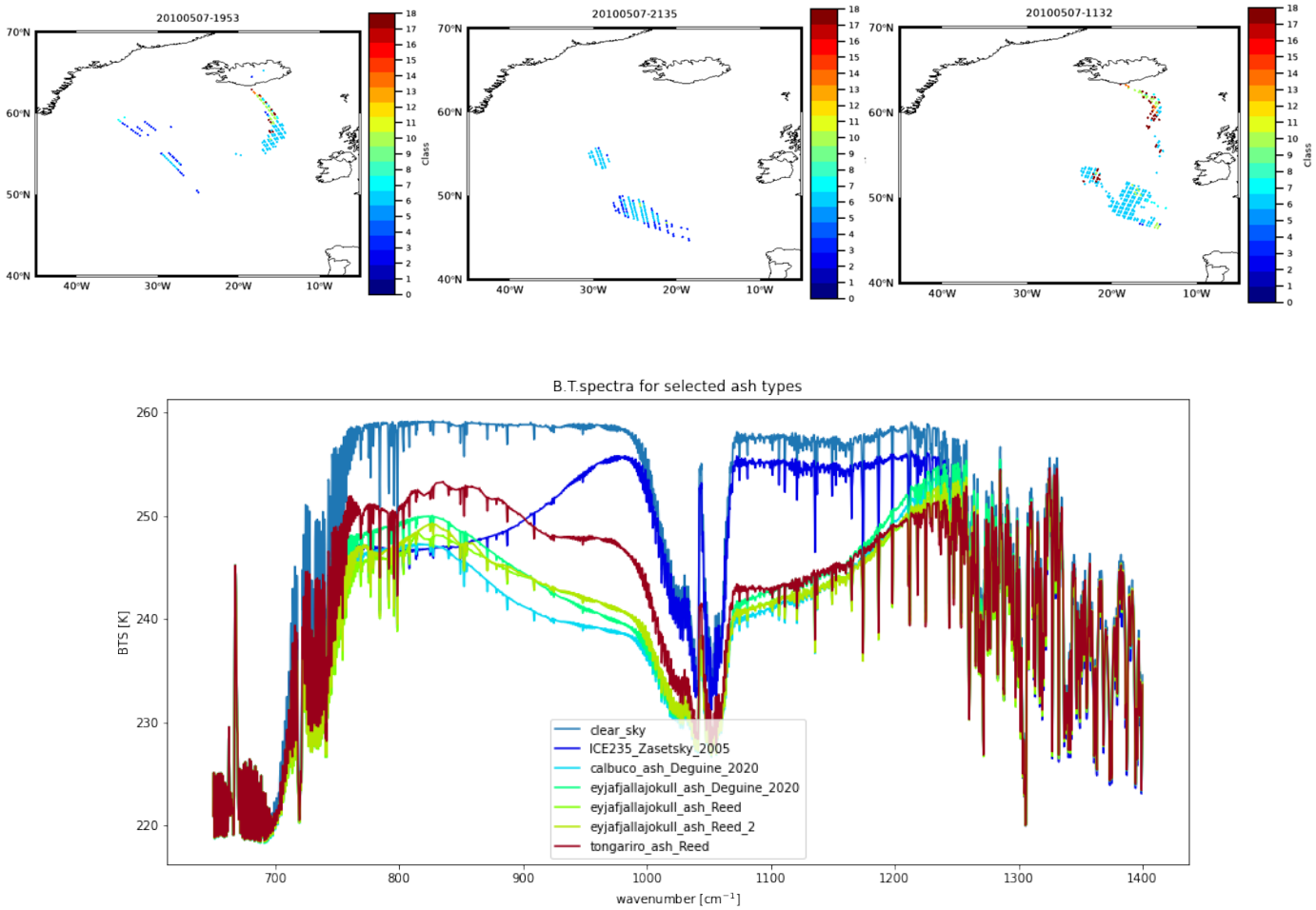

Figure 5: Application of the model (with scalar integer labels) on an Eyjafjallajökull eruption. Labels 9-11 represent various historical Eyjafjallajökull datasets, see Table (2). Dark blue dots (class 3) represent ice. Light blue dots (class 6) represent the LUT "calbuco_ash_Deguine_2020, a basaltic-andesitic volcano with not too different SO_2 content. Dark red ones correspond to class 18 (class 16 in Table (2)), which is "tongariro_ash_Reed", yet another andesitic volcano. These are not too far away from Eyjafjallajökull in terms of chemical composition, see more in the text. The bottom figure is a particular example of simulated spectra corresponding to these often chosen classes mentioned here. just mentioned, plotted for the same parameters as Figure (8)

.

what is the desired use of the model and fit the dataset selection and training strategy to this intended use. One possibility is to make a robust model, featuring also a range of surface emissivity types, atmospheric profiles and possibly other relevant parameters. Encompassing *all* the possible variations would allow the intended users to generate predictions to any TIR spectrum in principle in a fraction of a second (although some manual data pre-processing might be needed). However, this dataset would necessarily have coarser resolution in its parameter space, and might be just too large to handle computationally, for any reasonable coarsening of parameter space. Dataset that we used for training was already quite coarse, and it was limited to just one particular type of surface and atmosphere. In practice, a more viable path might be to scrap variations of all parameters that might be known in an experimental situation. Apart from atmospheric and surface types, we can also eliminate surface temperature. The truly unknown parameters that we used would be only the particle effective radius, the optical depth and the height of the plume in the atmosphere. This is all assuming that a potential user would be armed with the full TIR spectrum, as well as geographical coordinates and an appropriate database of meteorological data. This would however mean that an appropriate model would be needed for every volcanic observation separately.

- data processing:

  See whether there are modifications to spectra that can increase the model performance by removing noise. As a first step, high wavenumber ($> 1250cm^{-1}$ region of the spectrum, heavily influenced by water vapour absorption, has been removed from our study. Further modifications might include smoothing/removing gas spectral lines. This might not be necessary, since the model might filter out these features by itself - they are present in each spectrum regardless of the ash type.

- improve the model to do regression instead of classification:

  Currently the model spots a pattern in the data and assigns it to the nearest chemical composition cathegory. Ideally, it would be able to locate the ash in the plane of Figure (1), i.e. have some numerical output - albeit possibly imprecise.

- test on more real world data:

  The results so far seem reasonable, but not very accurate. Applying the model more will reveal its performance in detail. More importantly, it might point to further setbacks that need to be adressed.

Acknowledgements

MODIS emissivity data and RTTOV radiative transfer code were used in this work. IASI data was made available courtesy of EUMETSAT. Simulation code for generating dataset was developed by members of Earth Observation Data Group at AOPP, University of Oxford. Free software, in particular Python with its scikit-learn and NumPy library, was used extensively. scikit-learn is a simple, efficient and free ML package that is based on the work that was started in 2007 as a Google Summer of Code project by David Cournapeau. Its first publication was as follows:

Scikit-learn: Machine Learning in Python, Pedregosa et al., JMLR 12, pp. 2825-2830, 2011

I would like to especially thank Dr Isabelle Taylor and Professor Roy Gordon Grainger for their guidance throughout the project.

Bibliography

Roberto Carniel and Silvina Raquel Guzmán (October 19th 2020). Machine Learning in Volcanology: A Review, Updates in Volcanology - Transdisciplinary Nature of Volcano Science, Károly Németh, IntechOpen, DOI: 10.5772/intechopen.94217. Available from: https://www.intechopen.com/chapters/73667

Alexandre Deguine, Denis Petitprez, Lieven Clarisse, Snævarr Gumundsson, Valeria Outes, Gustavo Villarosa, and Hervé Herbin, "Complex refractive index of volcanic ash aerosol in the infrared, visible, and ultraviolet," Appl. Opt. 59, 884-895 (2020)

Muller A.C., Guido S., Introduction to Machine Learning with Python, O'Reilly Media, Incorporated, 2018 (ISBN: 9352134575, 9789352134571)

Ishimoto, H., Hayashi, M., and Mano, Y.: Optimal ash particle refractive index model for simulating the brightness temperature spectrum of volcanic ash clouds from satellite infrared sounder measurements, Atmos. Meas. Tech. Discuss. [preprint], https://doi.org/10.5194/amt-2021-103, in review, 2021.
Picchiani, Matteo Chini, Marco Corradini, Stefano Merucci, Luca Sellitto, Pasquale Del Frate, F. Stramondo, Salvatore. (2011). Volcanic ash detection and retrievals using MODIS data by means of neural networks. Atmospheric Measurement Techniques. 4. 10.5194/amt-4-2619-2011.

B. E. Reed, D. M. Peters, R. McPheat, and R. G. Grainger, "The complex refractive index of volcanic ash aerosol retrieved from spectral mass extinction," J. Geophys. Res. 123, 1339–1350 (2018).

Shoji, D., Noguchi, R., Otsuki, S. et al. Classification of volcanic ash particles using a convolutional neural network and probability. Sci Rep 8, 8111 (2018). https://doi.org/10.1038/s41598-018-26200-2

Ventress, L. J., McGarragh, G., Carboni, E., Smith, A. J., and Grainger, R. G.: Retrieval of ash properties from IASI measurements, Atmos. Meas. Tech., 9, 5407–5422, https://doi.org/10.5194/amt-9-5407-2016, 2016

Appendices

A Additional graphs

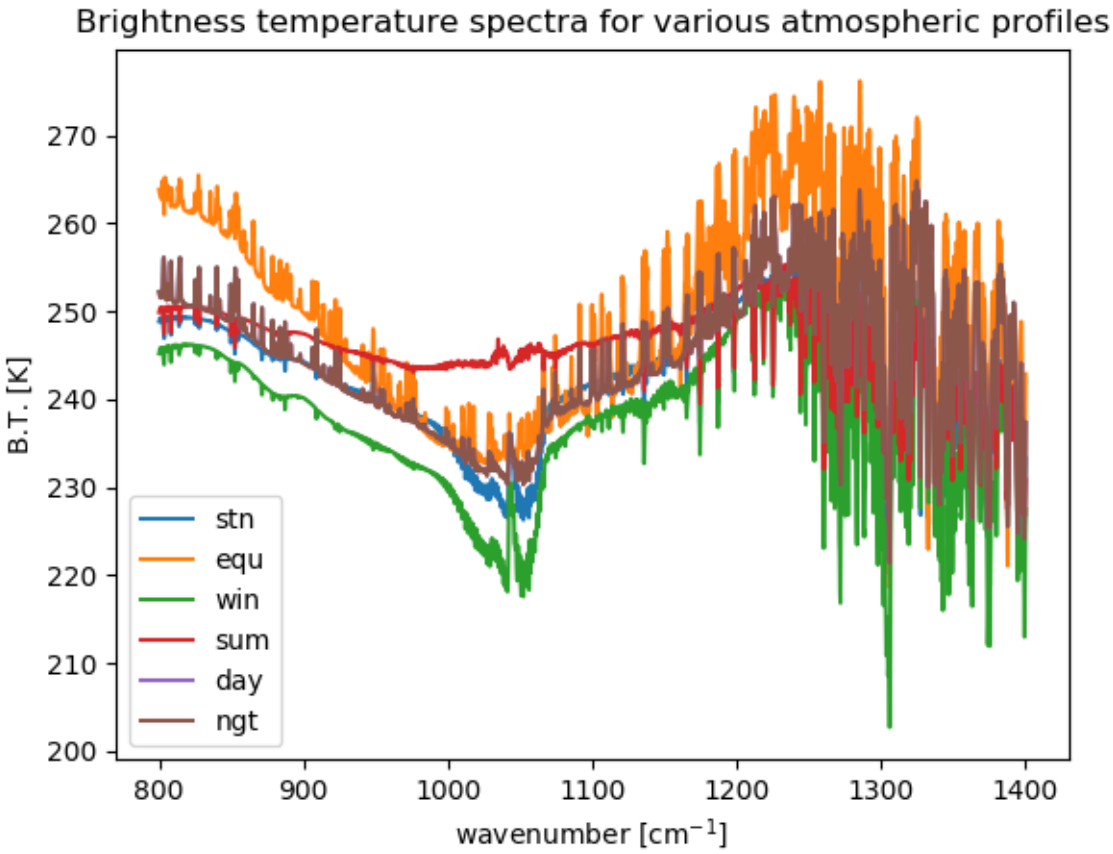

Figure 6: Brightness temperature spectra for the six atmospheric profiles used for generating the dataset.

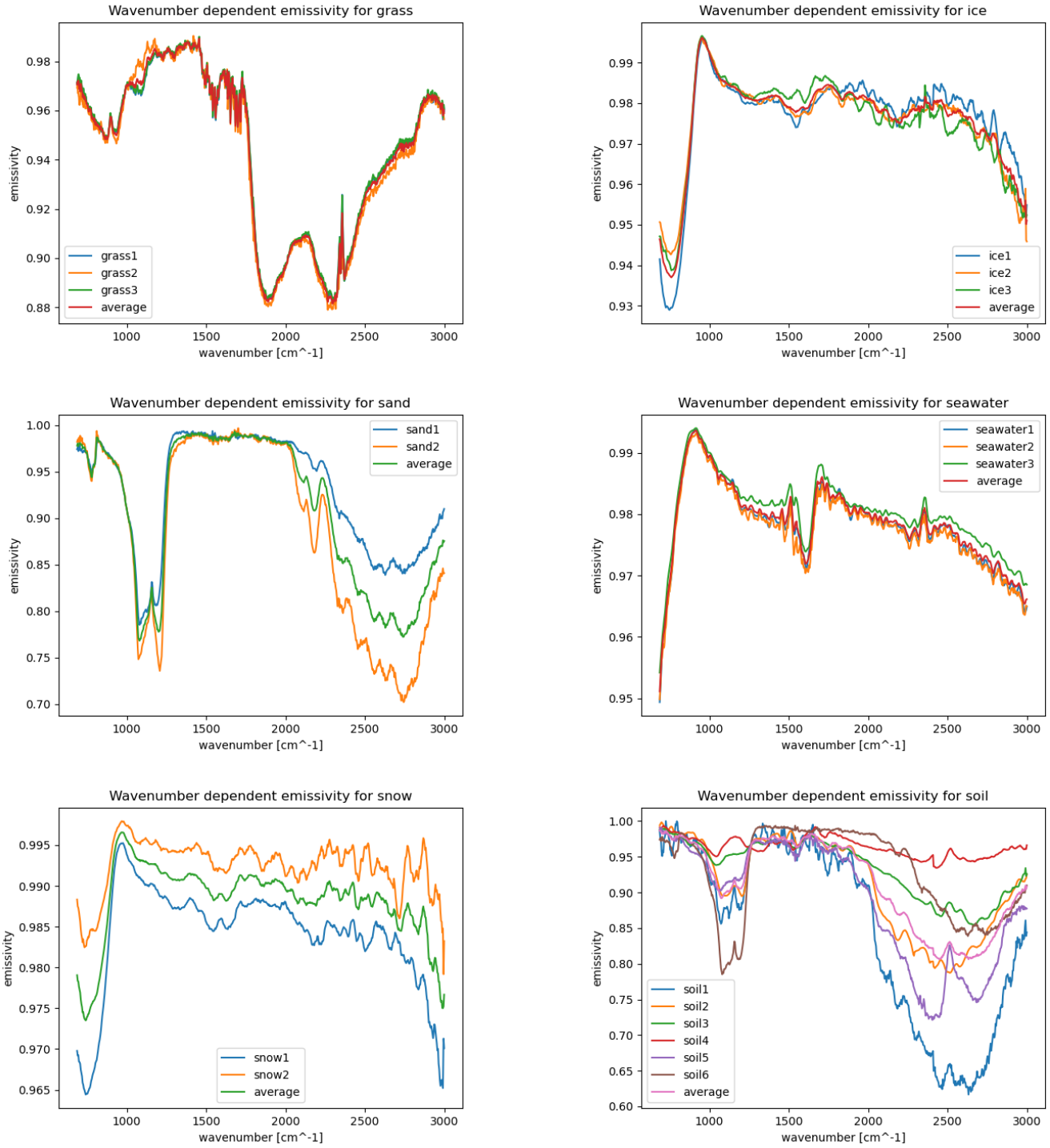

Figure 7: Emissivity datasets as taken from MODIS data.

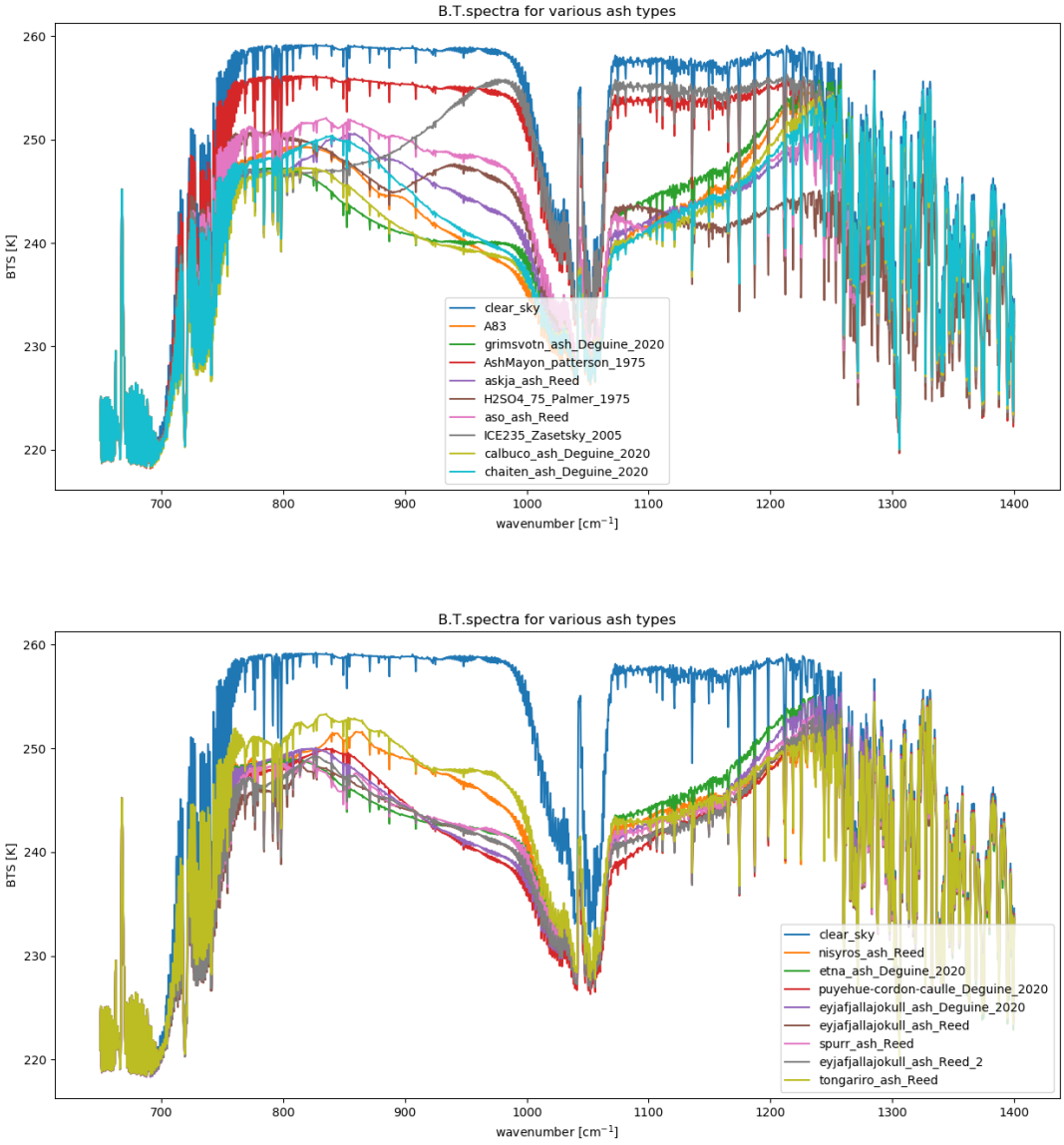

Figure 8: All 17 ash types used in the training of ML model, plotted for a particular fixed choice of remaining parameters. Two of "ash" types are actually not ash, but sulphuric acid and ice. Naming convention captures the name of the volcano, the year of eruption that was studied, and the name of the lead author of relevant study. The clear sky is added for reference.

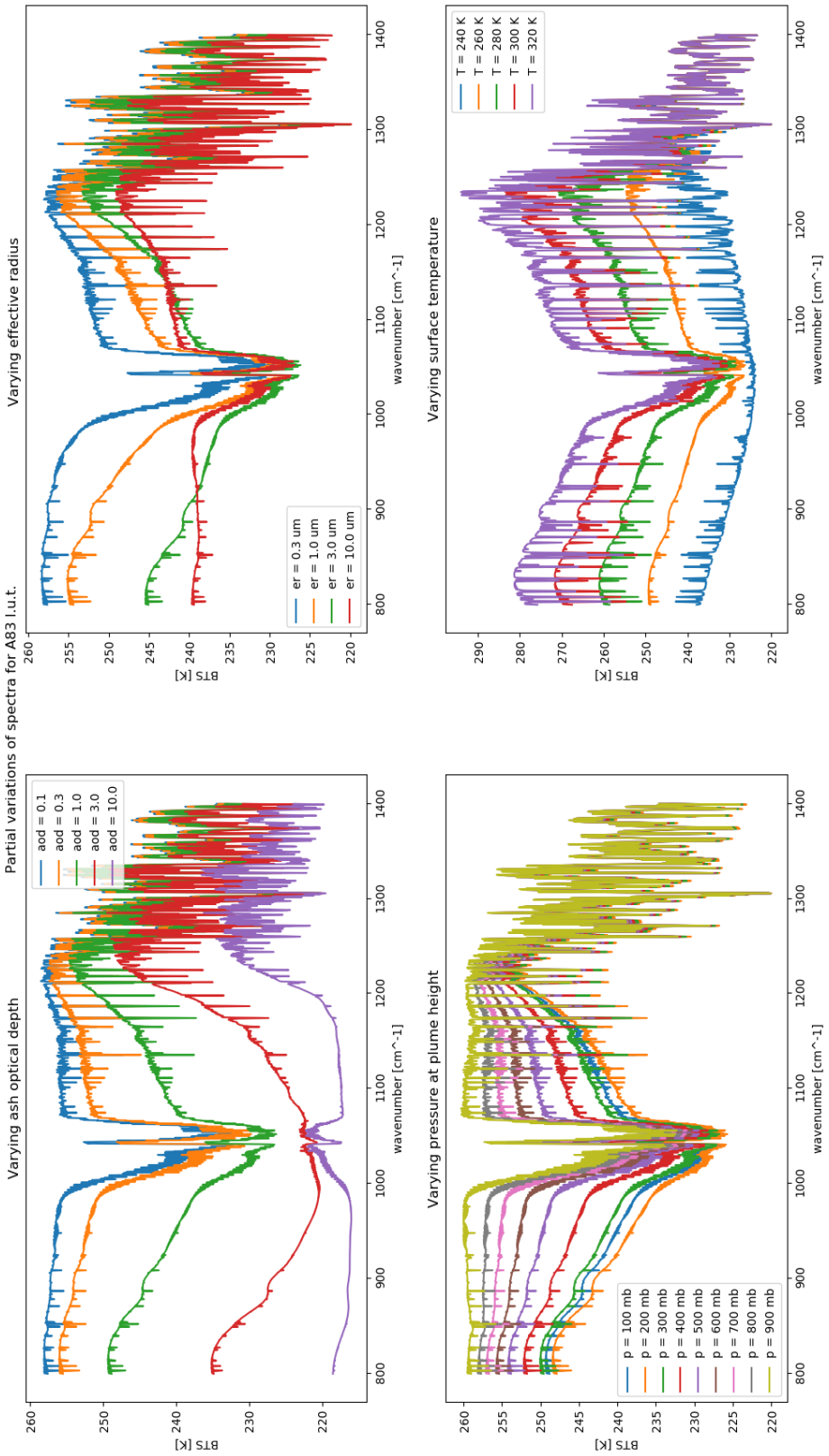

Figure 9: Partial variations with respect to four scalar parameters. Three of them are held constant, while the fourth one across its entire range. This is an example for one of the ash types (the look-up table 'A83').